Complex Pathways Drive Pluripotent Fmoc-Leucine Self-assemblies

Subir Paul+, Kousik Gayen+, Pau Gil Cantavella, Beatriu Escuder, Nishant Singh*

[a] Subir Paul, Kousik Gayen, Pau Gil Cantavella, Beatriu Escuder, Nishant Singh
Institute of Advanced Materials
Universitat Jaume I
Avinguda de Vicent Sos Baynat, s/n, 12006 Castelló de la Plana, Castelló, Spain
E-mail: nsingh@uji.es
+Equal contributions

Abstract: Nature uses complex self-assembly pathways to access distinct functional non-equilibrium self-assemblies. This remarkable ability to steer same set of biomolecules into different self-assembly states is done by avoiding thermodynamic pit. In synthetic systems, on demand control over 'Pathway Complexity' to access self-assemblies different from equilibrium structures remains challenging. Here we show versatile non-equilibrium assemblies of the same monomer via alternate assembly pathways. The assemblies nucleate using non-classical or classical nucleation routes into distinct metastable (transient hydrogels), kinetic (stable hydrogels) and thermodynamic structures [(poly)-crystals and 2D sheets]. Initial chemical and thermal inputs force the monomers to follow different assembly pathways and form soft-materials with distinct molecular arrangements than at equilibrium. In many cases, equilibrium structures act as thermodynamic sink which consume monomers from metastable structures giving transiently formed materials. This dynamics can be tuned chemically or thermally to slow down the dissolution of transient hydrogel, or skip the intermediate hydrogel altogether to reach final equilibrium assemblies. If required this metastable state can be kinetically trapped to give strong hydrogel stable over days. This method to control different self-assembly states can find potential use in similar biomimetic systems to access new materials for various applications.

Self-assembly pathways direct biomolecules to form distinct non-equilibrium structures. Albeit composed of same monomers, the functions and morphologies of such assemblies differ from their thermodynamically stable counterparts.[1]The high level of adaptivity in biological self-assemblies is achieved by navigating through different energy landscapes with several local minima before reaching thermodynamic equilibrium.[2] Such temporal control over versatile self-assemblies allows nature to avert synthesis of new molecules for different purposes. For example, Microtubules and Actin filaments are responsible for vital functions like cell stiffness, cell migration, and cell division. They can employ different coupling proteins to modulate their polymerization pathways which allow them to tailor their structures for required tasks.[3] Similarly, Exosomes can form different self-assemblies derived from single cell line like unilamellar vesicles, vesosomes, and tubular structures to serve different functions.[4] However, loss of control over competing pathways can also lead to unwanted structures like irreversible aberrant protein aggregation resulting in Alzheimer's and Parkinson's.[5]

Emulating such control over complex pathways to direct monomers for desired self-assembly outcomes remains challenging for Supramolecular chemists. Often they lead to untargeted self-assemblies. This warrants control over different kinetic and thermodynamic routes to access different metastable or equilibrium assemblies as needed. Since the seminal work by Meijer and co-workers,[1a] several contributions in the form of kinetic and thermodynamic models,[1b],[6] and experimental findings[1c],[7] have furthered our understanding to control competing self-assembly pathways- often termed as 'Pathway Complexity'. Managing these self-assembly pathways in biomimetic aqueous systems gets notoriously difficult as water competes for hydrogen bonding, and hydrophobic interactions become dominant.[7a-7c] Stupp and co-workers used peptide amphiphiles, and chromophore amphiphiles interacting via H- bonds and π orbital overlap respectively, to navigate through complex energy landscapes.[1b] They obtained controlled metastable, kinetically trapped or thermodynamic self-assemblies by changing the order of on and off switching of the competing interactions. Wilson and co-workers have used thermal ramps to switch inter-digitation of oligo-(ethylene glycol) chains in Janus dendrimers. Different kinetically trapped states rendered complex 3D assemblies like elongated, and compartmentalized 3D vesicles.[8]

Clearly, control over alternate assembly pathways can give access to new assemblies with distinct molecular arrangements, and properties moving away from equilibrium. In this regard, amino acids and peptide self-assemblies- widely used biomimetic scaffolds have not been subject to this approach extensively.[9] Perhaps owing to the challenges mentioned before. Like proteins in biological settings,[5] they show ability to phase separate by Liquid-Liquid- and Liquid-Solid phase separation (LLPS and LSPS).[9,10] Thus offering opportunity to explore alternative non-classical self-assembly pathways different from classical homogenous and secondary nucleation events. Pathway complexity control in such systems can lead to a new range of bio-inspired functional soft materials.

Here we present, multi-routed evolution of phase separated Fmoc-Leucine (FL) aggregates into hierarchical assemblies via complex self-assembly pathways (Scheme1:*Path1 to 8*). Initial conditions with set chemical and thermal cues

determine the self-assembly pathways and outcomes. The disordered phase separated FL aggregates (solidified droplets) can form metastable assemblies with different properties before reaching their final thermodynamic state. The metastable phase is usually a fibrous transient hydrogel with pathway dependent customizable lifetime (hours to days) and strength. The final thermodynamic states can be adjusted to different microscopic arrangements such as poly-crystal spherulites, or single crystals (*Path1&8*). The molecular packing differs for transient (polymorph B) and final assemblies (polymorph A). Interestingly, using instant pH switch or gradual pH switch, we can flip the order of appearance of metastable and thermodynamic assemblies by forcing them on distinct assembly pathways. These assemblies nucleate via non-classical, and classical pathways depending on the set conditions.[11] Instant pH increase results in non-classical nucleation (N-CN) of fibrillar hydrogel from solidified droplets within minutes. This is followed by slow solution crystallization (1d-3d) of free monomers to form crystals on the expense of hydrogel disassembly (Classical nucleation- CN) (*Path 8*). On the other hand, gradual pH change permits the accelerated nucleation of thermodynamically more stable polycrystals (within minutes). This is followed by the formation of metastable hydrogel only when the system increases to optimum pH levels (~1h). Here, both the distinct phases evolve directly from solidified droplets (N-CN) (*Path1*). Eventually, the polycrystals outgrow and consume the metastable hydrogel leading to its dissolution (~15h). If needed, the formation of transient hydrogel can be skipped all together accelerating the formation of polycrystals (~2h) (*Path2&3*). Furthermore, under set conditions the system evolves only to kinetically trapped hydrogel (polymorph B), which previously would give way to polymorph A (*Path6&7*). Therefore, we show complete control over complex assembly pathways of solidified FL droplets following classical and non-classical nucleation routes.

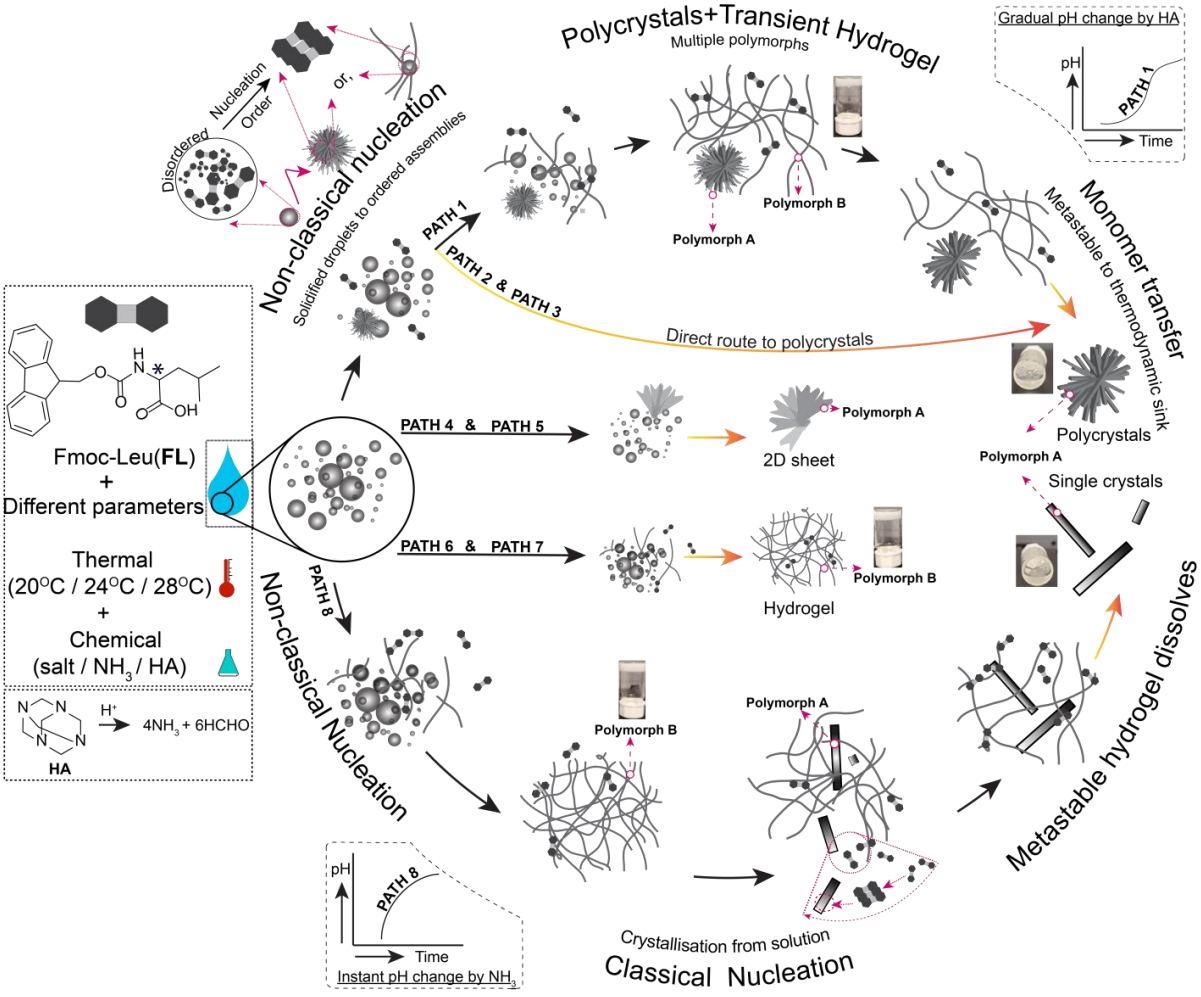

Scheme 1: General scheme depicting non-classical and classical nucleation routes for evolution of phase separated solidified droplets of FL. Path1 uses gradual pH change by HA hydrolysis to go through non-classical nucleation and give polycrystals (polymorph A), and transient hydrogels (polymorph B). Path 2 and Path 3 allow direct conversion of solid droplets to polycrystals without intermediate hydrogelation using thermal (high temperature) or chemical variations (no salt). Path 6 and 7 use chemical variations (salt with slow or fast pH change) to form stable kinetically trapped hydrogels with same molecular packing as transient hydrogel in Path 1. Path 8 is carried using instant pH change by NH_3 shot leading to instant gelation. The monomer rich solution then crystallizes to form single crystals (polymorph A)- classical nucleation. This results in dissolution of starting polymorph B hydrogel.

We selected amphiphilic FL as self-assembling motif for our studies based on previous reports on its self-assembling propensities. Draper et al realized an extensive study on gelation and subsequent crystallization of Fmoc-amino acids.[12] They found that FL gelation was not possible by pH change from basic to neutral/ acidic using Gluconolactone hydrolysis. Similarly, thermal annealing was ineffective for FL hydrogelation.[13] Solvent switch results in FL self-assembly into crystalline spherulites (water added to FL in MeOH).[14] In other very interesting study, Knowles, Yan, and co-workers[10b] report that FL can form phase separated droplets which solidify and subsequently form nanofibers. The fiber nucleation occurred in the metastable solidified droplets. This two-step nucleation event involving a less ordered pre-nucleation step is in line with non-classical nucleation theory (N-CN). It differs from classical single-step nucleation theory (CN) which assumes that ordered nuclei form directly from supersaturated solutions of monomers.

These different reports of FL self-assemblies make it a worthy candidate to explore complex assembly pathways in order to attain new structures and soft-materials. To test this, we set out to use phase separation (LLPS/LSPS) by solvent switch method using water+MeOH to explore the N-CN route for our studies. We wanted to avoid concentrated basic solution for FL dissolution to prevent unwanted Fmoc- deprotection (SI Fig. S1).[12] Another important factor is the FL concentration to improve our chances in achieving hydrogel like soft materials. Knowles and Yan report[10b] that increasing the monomer concentration led to accelerated liquid→solid droplets→fiber transitions (slowest for FL needing 1-2 months). Draper et. al. were unable to attain hydrogel with ~19mM of FL.[12] Considering the self-assembling timeframe and behavior in these reports, we decided to use higher FL concentration [~2 times- ~33mM].

Under these set conditions, clear methanol solution of FL immediately becomes turbid upon addition of water at 24^{o}C. Within 60 minutes, these aggregates grow and sediment leaving clear solution at the top (SI Fig. S2). Salts can decelerate or accelerate such transitions in phase separated systems. [10b,15] Therefore, we repeated same experiment by adding aqueous salt solutions to FL solution in MeOH. High salt ratios accelerated the previous transition 30 minutes (FL:Salt-1:5.1, 1:3.4, 1:1.7). whereas lower ratios (1:0.85, 1:0.42) behaved like salt-less system. Only exceptions were in presence of PO_4^{3-} where solutions remained clear with higher ratios. With lower ratios initially turbid solutions sometimes transformed into weak hydrogels. This behavior prompted us to check the pH of the systems.

We found that systems with high PO_4^{3-} ratios were above pH-8 causing FL dissolution. For lower ratios of PO_4^{3-} showing FL gelation the pH was 5.8-7.2, still higher than all other systems (pH3.8-5.2) (SI Fig. S3-S5). Over all, presence of salts visibly accelerated aggregation in these systems. Additionally, behavior with PO_4^{3-} alluded towards key role of pH changes in realizing self-assembly transitions via distinct pathways. Moving ahead, we decided to use $NaClO_4$ for experiments with two different ratios- 1:1.7(high salt ratio), and 1:0.42 (low salt ratio). Building up on observations with phosphate salts we checked for systems' response under controlled pH increase. We employed two ways to bring pH changes, instant pH change by addition of NH_3 shot to phase separated FL, and by slow hydrolysis of Hexamine (HA) to produce NH_3 *insitu* (Scheme 1). HA can hydrolyze in water and acidic media to form formaldehyde (HCHO) and ammonia (NH_3), we suspected that acidity of the system would be enough to carry out this hydrolysis. [16] After testing different concentrations we settled for set ratios of FL with NH_3, and HA to give desired pH change (6.0-7.0).

Addition of NH_3 to phase separated FL (equilibrated for 1 minute) resulted in formation of a very strong white hydrogel within 2-3 minutes from an initially turbid solution. The observations were similar even in presence of $NaClO_4$. HA on the other hand didn't show similar transformations (HA was dissolved in water with/without $NaClO_4$ and added to FL solution at t-0). For HA only, the initially turbid solution became clear within an hour and small transparent granules were observed at vial's bottom. However, at high salt concentration (1:1.7), the system transformed within minutes into a strong white hydrogel. For lower salt ratio (1:0.42), only after 50 minutes a hydrogel capable of supporting its weight was formed by inverted vial test. Interestingly, this hydrogel got weaker over time and completely disappeared within 9 hours, leaving behind granular structures similar to system with HA only. In other cases (high salt+HA and high/low salt+NH_3), the hydrogels were stable for over 5 days except when hydrogel was formed only by using NH_3. In this case, most of the hydrogel disappeared over 1-3 days leaving crystalline needles behind (SI Fig. S2).

These systems were then checked for self-assemblies using transmitted light microscopy and scanning electron microcopy (SEM). The initially turbid solutions of phase separated FL, with and without salt, were composed of poly-dispersed opaque particles (0.1-6µm). Soon after, we could observe formation of translucent 2D pleated sheets at the expense of disappearing particles. These thin sheets kept on growing over several mm^2 until all the particles had disappeared (SI Fig. S6a-S6e). SEM images revealed that these sheets were formed of closely aligned <1µm broad 2D fibers (SI Fig. S6f-S6k). Unlike previous reports of 1D fiber[10b] or flower shaped structures, [14] these 2D sheets could be a result of high FL concentration in line with previous reports on such concentration dependent sheets formation. [17] In other case, NH_3 mediated instant pH change resulted in immediate fiber formation (<1 µm). (Fig. 2e-I3, Fig. 3e-3f) We observed that these fibers originated from the phase separated particles, in line with non-classical nucleation (N-CN) observations reported before (Fig. 2a-2d, Inset I1 and I2, SI Video SV1). [10b] Notably, immediate vicinity of fibers showed obvious depletion in particle density when compared to regions without fiber presence. Within minutes, the system transitioned to densely packed fiber network corresponding to the macroscopic hydrogel formation before. Following through, we observed sporadic presence of crystals in fiber network after several hours. Eventually, the fibers

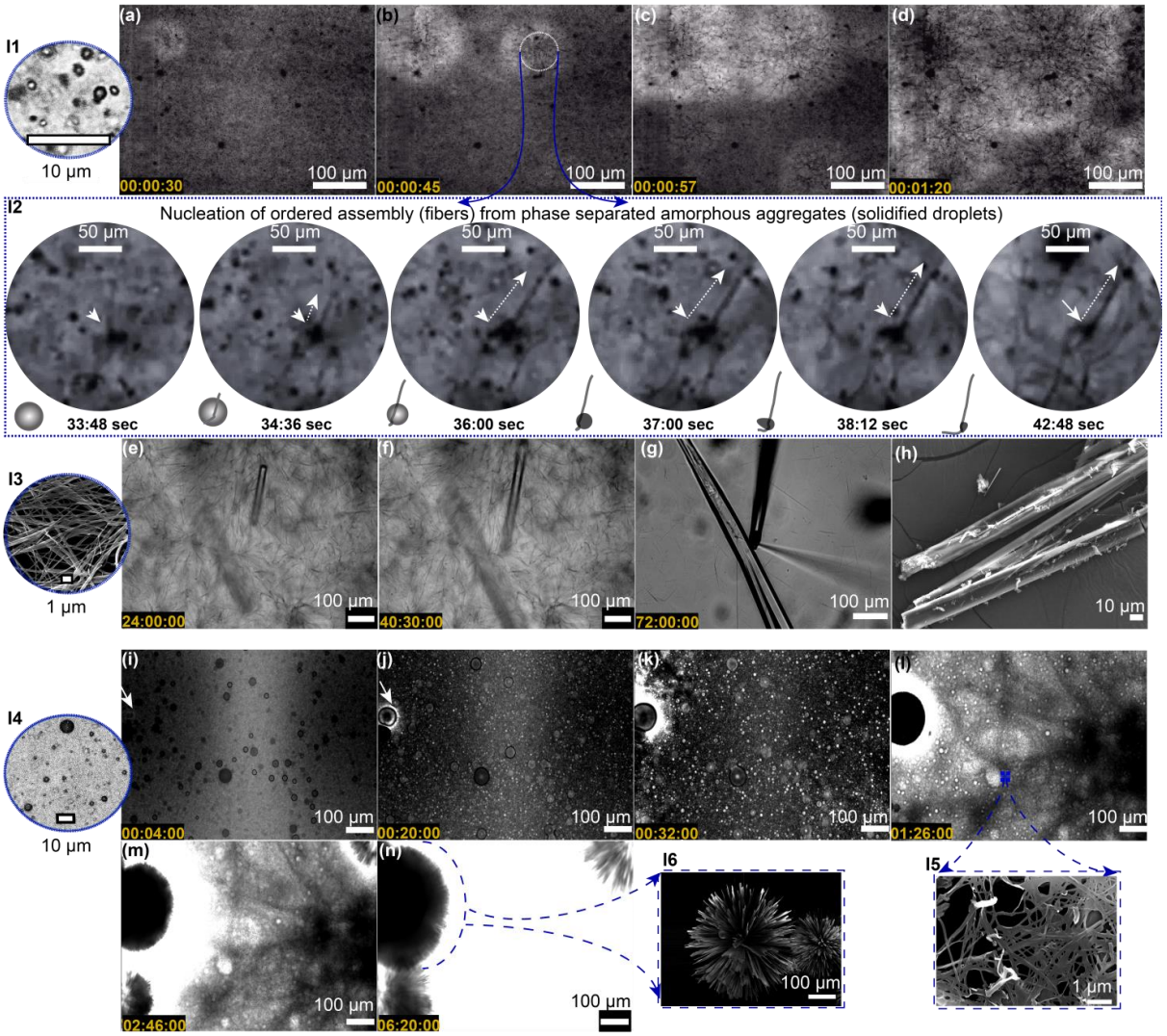

Figure 2: (a-d) FL+NH_3: Instant fiber formation via non-classical nucleation from solidified droplets. Inset I1 shows higher magnification image of the submicron sized initial aggregates. Inset I2 shows direct observation of fiber nucleation from them. (e-g) FL+NH_3: Crystal growth in solution to form long crystals over 3 days, leads to fiber dissolution. Inset I3 shows SEM images of the fibers (h) SEM image of the crystals.(i-j) FL+Salt(1:0.42)+HA: Nucleation of polycrystals from phase separated particles (white arrows show nucleation point). Inset I4 shows higher magnification image of mostly submicron sized initial aggregates. (k-l) Formation of transient hydrogel network. Inset I5 shows SEM images of the fibers (m-n) Fibers disassemble leaving large sea urchin shaped polycrystals. Inset I6 shows SEM images of polycrystals. The inset drawings are not to scale. Also see supporting videos. Time format- hr:min:sec.

totally disappeared leaving the crystals behind. Interestingly, even when these crystals almost tripled in size the fibers surrounding them seemed intact (Fig. 2e-2h, Inset I1 and I3). Unlike the particle to fiber transition, this alludes that fibers are not directly involved in crystal formation but crystallization may happen from soluble monomers via CN- typical of Ostwald ripening. [17d] We then looked into FL system showing similar transitions with gradual pH change with low salt(1:0.42)+HA. Within minutes sea urchin like assembly nucleated from initial turbid solution composed of particles. These rigid looking structures composed of needle like fibers grew denser and bigger in size by consuming particles around them (Fig. 2i-2k, Inset I4). 20 minutes later we see fibers emerging from the particle rich areas leading to total disappearance of particles. The system now has crystalline and rigid sea urchin like assemblies along with several millimeter long wavy fibers (Fig. 2k-2l, Inset I5). However, the crystalline assemblies continue to grow while the fibers disassemble. Finally, large rigid assemblies composed of thick crystalline fibers (polycrystals) are left behind (Fig. 2m-2n, Inset I6, SI Video SV2). In case with high salt ratio(1:1.7)+HA, the fiber network formed within minutes and were concentrated in adjoining patchy domains (SI Fig. S7b). We could not spot polycrystals as in previous low salt+HA case. These fibers remained unchanged over three days unlike the system with lesser salt (SI Fig. S7a). Note: Coalescence is characteristic of droplets after LLPS but we don't see such fusion of particles here. Centrifuging the turbid solutions resulted in solid sediments and clear supernatant instead of forming two liquid phases(SI Fig. S8).[15, 18] It could be that droplets solidify instantly at such high [FL] in line with previously observed solidification kinetics. [10b]

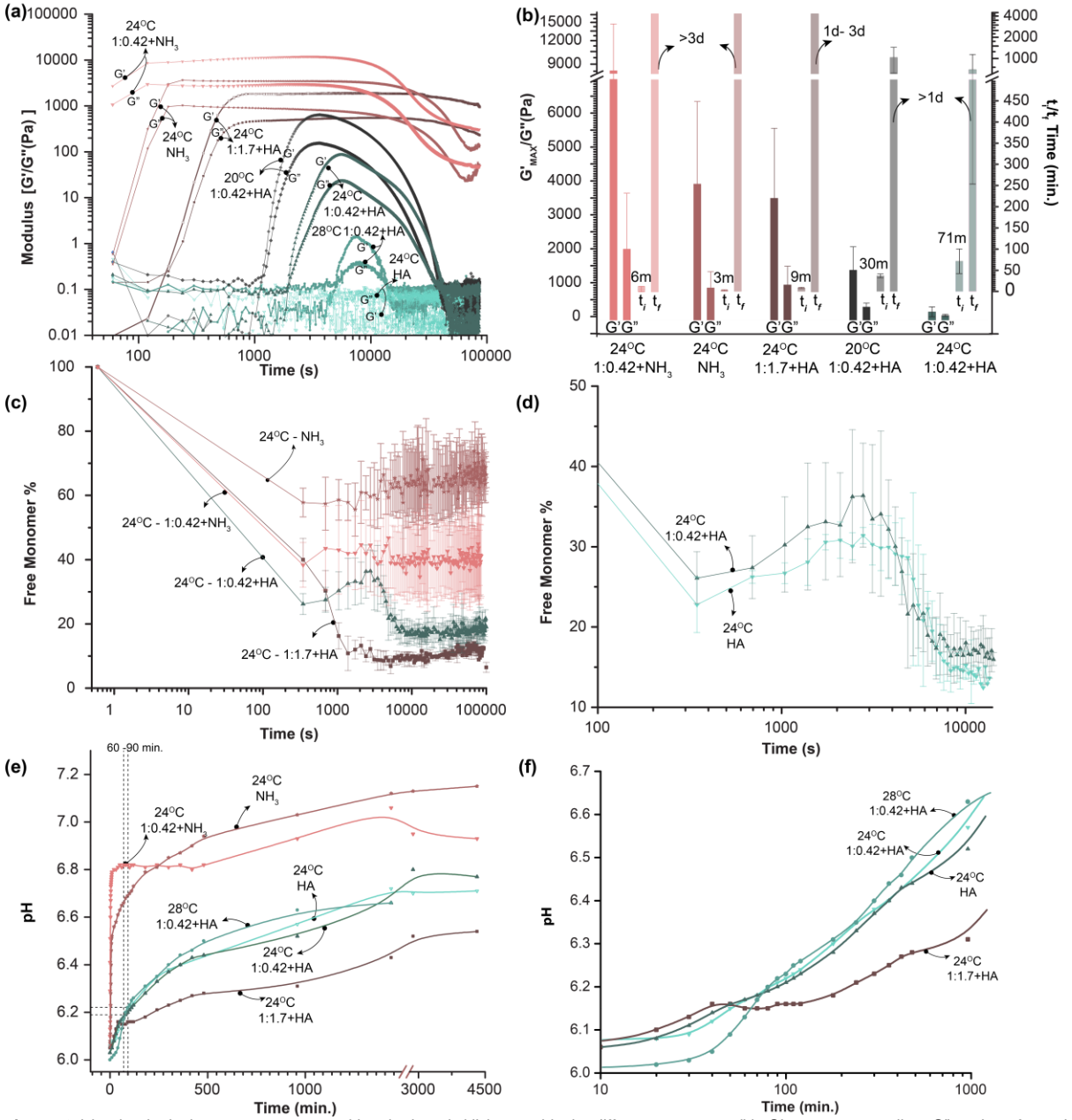

Figure 3:(a) Rheological measurements tracking hydrogel (dis)assembly in different systems. (b) G'_{max}, corresponding G", t_i-time for gel formation, and t_f- time for gel dissolution for different systems. (c) ^{1}H NMR kinetics experiments to track free monomer concentration over 24 hours for different systems. Set quantity of hydroquinone dissolved in D_2O was used as external reference; completely solubilized FL (using NH_3) at working concentration was used to measure 100% free monomer concentration. (d) Monomer concentration comparison over time for FL+ -HA and -HA+low salt system. (e) pH profile over 3 days for different systems. Dotted lines show 60-90 min region crossing over at pH-6.2. (f) Zoomed in pH profile of different closely overlapping systems with HA.

We then checked the mechanical response of these systems using rheology (Fig. 3a&3b, SI Fig. S11-S17). FL hydrogels with NH_3 and Salt(1:0.42)+NH_3 were quickest to form (t_i<6 min, t_i-time of gel initiation when G'=0.5G'_{max}). Salt(1:0.42)+NH_3 reached G'_{max} of ~9000 Pa, and NH_3 hydrogel showed G'_{max} of ~3500 Pa. In both the cases the gel strength reduced over time due to formation of crystals and fiber dissolution. Salt(1:1.7)+HA system also formed relatively strong gel with G'_{max} of ~3000 Pa and t_i-9 min. This gel showed very little depreciation in its mechanical strength over 24 hours. The patchiness of fibrous self-assemblies could lead to ineffective holding of gel together leading to the observed decrement (SI Fig. S6b). Salt(1:0.42)+NH_3 system showed interesting transient gelation behavior at 24^{O}C reaching G'max- of ~80 Pa in around 70 minutes. This hydrogel took ~15 hours' to disassemble (t_f). We then checked if temperature variations could impact the hydrogel (dis)assembly dynamics. At 20 ^{O}C, the t_i reduced to ~30 min with higher G'_{max} ~1000 Pa and taking 3 hours longer for dissolution. At 28 ^{O}C, no hydrogel formed (G'-G"<5Pa) which was similar to system with HA only. In both these cases the solidified droplets transformed into polycrystals by skipping transient hydrogel formation. (Fig. 3a&3b, SI Fig. S9, SI Video SV3, SV4, SV5).

https://doi.org/10.26434/chemrxiv-2024-l2lt7 **ORCID:** https://orcid.org/0000-0003-2218-566X

Next we performed ^{1}H NMR kinetic experiments to follow different self-assembly pathways (Fig. 3c, SI Fig. S18-S24). For simple FL in water and FL+low salt(1:0.42) system no free monomers were visible by NMR (hard to quantify). This suggests that the droplets solidify instantly(<5 minutes) and the subsequent transition to fiber and sheets is directly from them via N-CN (SI Fig. S18-S19). For NH_3 case, the free monomers% was around 58% after 15 min. In presence of salt, this dropped to ~42%. In next 24 hours, we observe major fluctuations in these two cases giving big error bars. Stochastic crystallization of the soluble monomers can cause big differences in independent experiments. Crystallization will reduce soluble monomers causing dissolution of fibers to re-equilibrate the monomer concentration leading to such differences. Especially for NH_3 case, such saturated solution with high monomer concentration is likely to favor classical nucleation. We also observe a gradual increase in free monomer from 58% to. 68% in 24 hours in case of NH_3, whereas NH_3+salt remains in the 42-45% range. The dissolving fibers should become less capable of withholding the monomers in assembled state. This would result in solution with higher monomer concentration than when hydrogel was intact in return speeding up the crystallization process. After three days when crystallization is complete, the free monomer% for NH_3 decreases significantly but not for NH_3+salt (SI Fig. S24b). Few small crystals also appear in Salt(1:0.42)+NH_3 case but this doesn't lead to hydrogel dissolution. Clearly, salt is able to reduce the repulsion in deprotonated FL allowing higher contribution in self-assembly which also evident from the pH profiles (NH_3>salt+NH_3 after 5h). For Salt(1:0.42)+HA, the free monomer% was around 30% in first 15 minutes. The latent NH_3 release by HA should deprotonate and solubilize FL slowly and allow more protonated monomers to stay aggregated (HA, and NH_3 systems need ~60min., and ~2 min. respectively to reach 6.3.- Fig. 3e&3f). Eventually, the monomer concentration increases from ~28% to ~38% in next 60-90 minutes. This coincides with hydrogel formation in this system. If we compare this with FL+HA system with fewer fibers, we find overlapping pH profiles but 10% lesser free monomer% (Fig. 3d, Fig. 2i-2l, SI Fig. S9). Clearly, salt favors the formation of 1D fiber assemblies leading to hydrogel. This also hints that fibers are composed of higher number of deprotonated FL molecules. Lastly, Salt(1:1.7)+HA showed quick drop in free monomer concentration to below 10% within 15 minutes. Again, high salt concentration not only favors rapid 1D assembly but also involves more deprotonated monomers in fiber formation. This is evident from the pH profile which remains much lower than other systems involving HA (Fig. 3e&3f, SI Fig. S7).

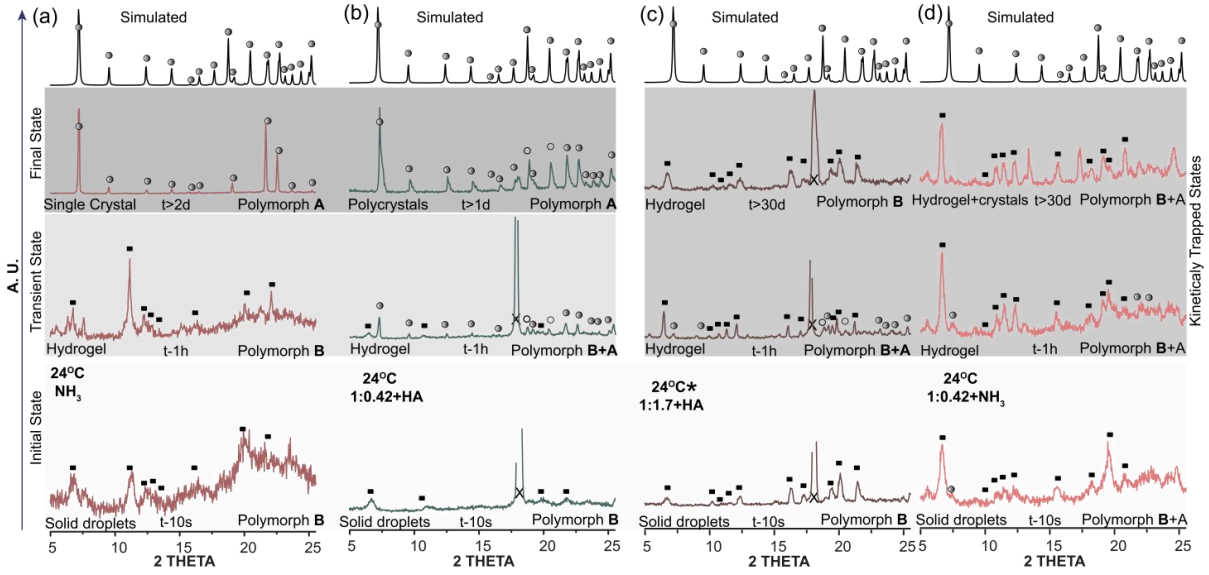

Figure 4: Powder XRD patterns of FL self-assemblies at set stages in different assembly pathways (Initial solidified droplets, transient/metastable hydrogel, kinetically trapped hydrogel and final crystals and polycrystals). Two major polymorphs are observed; depicted by circle- polymorph A, and rectangles- polymorph B. Simulated powder XRD from single crystal data[19] of Fmoc-L-Leu is shown at the top of each panel. (a) FL+NH_3 system at 24^{O}C, (b) FL+low salt+HA at 24^{O}C, (c) FL+high salt+HA at 24^{O}C, (d) FL+low salt+NH_3 at 24^{O}C.Peaks marked with X are from HA±Salt additives.

We then checked for powder XRD patterns to compare molecular packing in the different self-assemblies (Fig. 4, S25-S28, Table S1). For NH_3 driven system, the final crystals of FL(L) were suitable to be resolved by single crystal XRD. However, the crystal structure of this molecule is already reported.[19] We back simulated the powder XRD pattern of pure crystal phase and used it to compare crystallinity and polymorphism of other self-assemblies (SI Fig. S32). In all the cases, the initial turbid phase composed of solidified droplets showed patterns with broad peaks and noisy baseline characteristic of amorphous less ordered packing.[20] This is even more evident when patterns for initial phase are compared with the forthcoming stages (Transient/Final/Kinetically trapped states) (Fig. 4). The later stages in general show better resolved peaks alluding toward more ordered packing. For NH_3 system, initial solid droplets and transient gel phases showed different polymorph (rectangles- polymorph B) than the final single crystal phase (circles- polymorph A) (Fig. 4a, Table S1). For Salt(1:0.42)+HA, initial solid droplets poorly diffract pattern similar to polymorph B (Fig. 4b). However, during the transient hydrogel phase two polymorphs can be recognized (A+B). polymorph A and polymorph B

can be assigned to hydrogel fibers and polycrystals, respectively. Eventually the metastable polymorph B disappears, and the final pattern for polycrystals perfectly matches for Polymorph A. The peaks although sharp are much broader at base which could be due to several crystals present in one structure (polycrystals).[20] Polycrystals from HA, and from 28^{O}C high salt(1:1.7)+HA systems corresponded to polymorph A (SI Fig. S28). In the two kinetically trapped systems, polymorph B characteristic of 1D fiber assembly is dominant, some amount of polymorph A can also be detected (Fig. 4c-4d). But unlike the systems with metastable hydrogels, here polymorph A is unable to clean up polymorph B even after 30 days. This is more evident in the case with high salt(1:1.7)+HA where in fact polymorph A disappears overtime (Fig. 4c). Together with microscopy, pH, and NMR studies this could mean that polymorph B fibers have higher contributions from deprotonated FL when compared to thermodynamically stable polymorph A crystals.

In summary, we show how complex pathways can lead to differences in molecular packing via non-classical or classical nucleation to form distinct self-assemblies with different macroscopic properties. The different (dis)assembly pathways and kinetics of FL are based on combined effect of pH with important contributions from other chemical and thermal components. Kinetics of pH change, and salt concentrations directly impact hydrogelation kinetics and stability giving distinct polymorph than the thermodynamic one. We see that salts in optimum pH range promote 1D fiber networks by incorporating more deprotonated molecules. This leads to kinetically trapped or transient hydrogels with distinct lifetime and mechanical strength. Absence of salt favors the system to reach equilibrium faster forming thermodynamic assemblies. Similarly, by temperature perturbations we can favor thermodynamic assemblies and preclude metastable ones or vice-versa. Therefore, by introducing complex self-assembly pathways we show complete control over evolution of metastable, kinetic and thermodynamic self-assemblies. This can potentially be translated to other similar biomimetic systems for tailored applications.

Acknowledgements

NS, KG and PG would like to acknowledge the support from Generalitat Valenciana (Conselleria de Innovación, Universidades, Ciencia y Sociedad Digital) for CIDEGENT PlaGenT grant no. CIDEXG/2022/16 for the project PRONESS. NS acknowledges UJI for funding (UJI-2023-08). SP and BE thank UJI for funding (Grant UJI-B2020-21). We thank Servei Central d'Instrumentació Científica (SCIC) at Universitat Jaume I, Spain.

Keywords: Pathway complexity • Non-classical nucleation • non-equilibrium • supramolecular • soft-materials

References

1] a) P. A. Korevaar, S. J. George, A. J. Markvoort, M. M. J. Smulders, P. A. J. Hilbers, A. P. H. J. Schenning, T. F. A. de Greef, E. W. Meijer, *Nature* **2012**, *481*, 492–496; b) F. Tantakitti, J. Boekhoven, X. Wang, R. V. Kazantsev, T. Yu, J. Li, E. Zhuang, R. Zandi, J. H. Ortony, C. J. Newcomb, L. C. Palmer, G. S. Shekhawat, M. O. de la Cruz, G. C. Schatz, S. I. Stupp, *Nat.Mater***. 2016**, *15*, 469 –47; c) T. Fukui, S. Kawai, S. Fujinuma, Y. Matsushita, T. Yasuda, T. Sakurai, S. Seki, M. Takeuchi, K. Sugiyasu, *Nat. Chem.* **2017**, *9*, 493 –499; d) F. J. Rizzuto, C. M. Platnich, X. Luo, Y. Shen, M. D. Dore, C. Lachance-Brais, A. Guarné, G. Cosa, H. F. Sleiman, Nat. Chem. 2021, 13, 843-850; e) E. te Brinke, J. Groen, A. Herrmann, H. A. Heus, G. Rivas, E. Spruijt, W. T. S. Huck, *Nat. Nanotechnol*. **2018**, *13*, 849 –855.
[2] K. Das, L. Gabrielli, L. J. Prins, *Angew. Chem. Int. Ed.* **2021**, *60*, 20120– 20143.
[3] M. Dogterom, G. H. Koenderink, *Nat. Rev. Mol. Cell Biol.* **2019**, *20*, 38-54.
[4] D. Zabeo, A. Cvjetkovic, C. Lasser, M. Schorb, J. Lotvall, J. L. Hoog, *J. Extracell. Vesicles,* **2017**, *6*, 1329476.
[5] a) E. T. Powers, D. L. Powers, *Biophys. J.* **2006**, *91*, 122–132; b) E. T. Powers, D. L. Powers, *Biophys. J.* **2008**, *94*, 379–391; c) W. S. Gosal, I. J. Morten, E. W. Hewitt, D. A. Smith, N. H. Thomson, S. E. Radford, *J. Mol. Biol*. **2005**, *351*, 850 –864; d) F. Hasecke, T. Miti, C. Perez, J. Barton, D. Schçlzel, L. Gremer, C. S. R. Grüning, G.Matthews, G.Meisl, T. P. J. Knowles, etal., *Chem. Sci.* **2018**, *9*, 5937 –5948.
[6] a) M. Becchi, R. Capelli, C. Perego, Giovanni M. Pavan, Cristian Micheletti, *Soft Matter*, **2022**, *18*, 8106-8116; b) G. Ghosh, *Giant* **2023**,*14*, 100160; c) D. van der Zwaag, P. A. Pieters, P. A. Korevaar, A. J .Markvoort, A. J. H. Spiering, T. F. A. de Greef, E. W. Meijer, *J. Am. Chem. Soc*. **2015**, *137*, 12677–12688; d) E. E. Greciano, B. Matarranz, L. Sunchez, *Angew. Chem. Int. Ed.* **2018**, *57*, 4697 –4701; e) W. M. Jacobs, A. Reinhardt, D. Frenkel, *Proc. Natl. Acad. Sci. USA* **2015**, *112*, 6313-6318; 6f) A. Mishra, D. B. Korlepara, S. Balasubramanian, S. J. George, *Chem. Commun*, **2020**, *56*, 1505-1508; 6g) Y. Chen, Y. Shi, Z. Gao, L. Wang, Y. Tang, J. Liu, C. Liu, *Angew. Chem. Int. Ed.* **2023**, *62*, e202302581.
[7] a) J. Deng, A. Walther, *J. Am. Chem. Soc.* **2020**, *142*, 685-689; b) P. A. Korevaar, T. F. A. de Greef, E. W. Meijer, *Chem. Mater.* **2014**, *26*, 576−586. c) M. F. J. Mabesoone, A. J. Markvoort, M. Banno, T. Yamaguchi, F. Helmich, Y. Naito, E. Yashima, A. R. A. Palmans, E. W. Meijer, *J. Am. Chem. Soc.* **2018**,*140*, 7810-7819. d) L. Borsdorf, L. Herkert, N. Bäumer, L. Rubert, B. Soberats, P. A. Korevaar, C. Bourque, C. Gatsogiannis, G. Fernández; *J. Am. Chem. Soc.* **2023**, *145*, 8882−8895. e) P. Khanra, A. K. Singh, L. Roy, A. Das, *J. Am. Chem. Soc.* **2023**, *145*, 5270−5284; f) I. Helmers, B. Shen, K. K. Kartha, R. Q. Albuquerque, M. Lee, G. Fernández, *Angew. Chem. Int. Ed.* **2020**, *59*, 5675 – 5682; g) R. K. Grötsch, C. Wanzke, M. Speckbacher, A. Angı, B. Rieger, J. Boekhoven, *J. Am. Chem. Soc.* **2019**, *141*, *25*, 9872–9878.
[8] J. Luan, D. Wang, S. Zhang, Y. Miyazaki, W. Shinoda, D. A. Wilson, *J. Am. Chem. Soc.* **2023**, *145*, 15496−15506.
[9] P. Zhou, R. Xing, Q. Li, J. Li, C. Yuan, X. Yan, *Matter* **2023**, *6*, 1945-1963.
[10] a) A. Levin, T. O. Mason, L. Adler-Abramovich, A. K. Buell, G. Meisl, C. Galvagnion, Y. Bram, S. A. Stratford, C. M. Dobson, T. P. J. Knowles, E. Gazit, *Nat. Commun*. **2014,** *5*, 5219. b) C. Yuan, A. Levin, W. Chen, R. Xing, Q. Zou, T. W. Herling, P. K. Challa, T. P. J. Knowles, X. H. Yan, *Angew. Chem., Int. Ed.* **2019**, *58*, 18116-18123.
[11] a) J. De Yoreo, P. U. P. A. Gilbert, N. A. J. M. Sommerdijk, R. L. Penn, S. Whitelam, D. Joester, H. Z. Zhang, J. D. Rimer, A. Navrotsky, J. F. Banfield, A. F. Wallace, F. M. Michel, F. C. Meldrum, H. Colfen, P. M. Dove, *Science* **2015**, *349*, aaa6760. b) M. Jehannin, A. Rao, H. Colfen, *J. Am. Chem. Soc.* **2019**, *141*, 10120-10136. c) Y. Tsarfati, S. Rosenne, H. Weissman, L.J. W. Shimon, D. Gur, B. A. Palmer, B. Rybtchinski, *ACS Cent. Sci.* **2018**, *4*, 1031-1036. d) X. Zhang, Crystallization via Nonclassical Pathways Volume 1: Nucleation, Assembly, Observation & Application, American Chemical Society, 2020.

[12] E. R. Draper, K. L. Morris, M. A. Little, J. Raeburn, C. Colquhoun, E. R. Cross, T. O. McDonald, L. C. Serpell, D. J. Adams, *CrystEngComm* **2015**, *17*, 8047–8057.
[13] a) Y. Xie, X. T. Qin, J. Y. Feng, C. Zhong, S. R. Jia, *J. Mater. Sci.* **2021**, *56*, 7626; b) I. Irwansyah, Y.-Q. Li, W. Shi, D. Qi, W. R. Leow, M. B. Y. Tang, S. Li and X. Chen, *Adv. Mater.*, **2015**, *27*, 648–654; c) Z. M. Yang, H. W. Gu, Y. Zhang, L. Wang and B. Xu, *Chem. Commun.*, **2004**, 208-209; d) Z. M. Yang, K. M. Xu, L. Wang, H. W. Gu, H. Wei, M. J. Zhang and B. Xu, *Chem. Commun.*, **2005**, 4414-4416.
[14] B. Koshti, H. W. A. Swanson, B. Wilson, V. Kshtriya, S. Naskar, H. Narode, K. H. A. Lau, T. Tuttle, N. Gour, *Phys. Chem. Chem. Phys.*, **2023,** *25*, 11522–11529.
[15] S. Kim, H. Y. Yoo, J. Huang, Y. Lee, S. Park, Y. Park, S. Jin, Y. M. Jung, H. Zeng, D. S. Hwang, Y. Jho, *ACS Nano,* **2017**, *11*, 6764-6772.
[16] N. Singh, B. Lainer, G. J. M. Formon, S. D. Piccoli, T. M. Hermans, *J. Am. Chem. Soc.* **2020**, *142*, 4083−4087.
[17] a) I. Insua, J. Montenegro, *J. Am. Chem. Soc.* **2020**, *142*, 300−307; b) S. Dhiman, R. Ghosh, S. Sarkar, S. J. George, *Chem. Sci.*, **2020**, *11*, 12701-12709; c) L. Wei, J. Lin, C. Chen, L. Yu, C. Lu, F. Liu*, Adv. Mater. Interfaces,* **2023**, *10*, 2202310; d) T. Jiang, C. F. Xu, Y. Liu, Z. Liu, J. S. Wall, X. B. Zuo, T. Q. Lian, K. Salaita, C. Y. Ni, D. Pochan, V. P. Conticello, *J. Am. Chem. Soc.* **2014**, *136*, 4300-4308.
[18] a) P. Mohammadi, A. S. Aranko, L. Lemetti, Z. Cenev, Q. Zhou, S. Vir-tanen, C. P. Landowski, M. Penttilä, W. J. Fischer, W. Wagermaier, M.B. Linder, *Commun Biol* **2018**, *1*, 86; b) T. Lu, E. Spruijt, *J. Am. Chem. Soc.* **2020**, *142*, 2905−2914; c) K. K. Nakashima, M. H. I. van Haren, A. A. M. André, I. Robu, E. Spruijt, *Nat. Commun*. **2021**, *12*, 3819.
[19] K. Yamada, D. Hashizume, T. Shimizu, K. Deguchi, *Acta Crystallogr.* E64, **2008**, o1112.
[20] a) S. Nasiri, M. Rabiei, A. Palevicius, G. Janusas, A. Vilkauskas, V. Nutalapati, A. Monshi, *Nano Trends* **2023**, *3*, 100015. b) T. Ungar, *Scripta Materialia,* **2004**, *51*, 777–781